



HAL
open science

Impact of past steel-making activities on lanthanides and Y (REY) fractionation and potential mobility in riverbank sediments

Christophe Hissler, Emmanuelle Montargès-Pelletier, Hussein Kanbar,
Mathieu Le Meur, Christophe Gauthier

► To cite this version:

Christophe Hissler, Emmanuelle Montargès-Pelletier, Hussein Kanbar, Mathieu Le Meur, Christophe Gauthier. Impact of past steel-making activities on lanthanides and Y (REY) fractionation and potential mobility in riverbank sediments. *Frontiers in Earth Science*, 2023, 10, pp.1-12. 10.3389/feart.2022.1056919 . hal-03932555

HAL Id: hal-03932555

<https://hal.univ-lorraine.fr/hal-03932555v1>

Submitted on 10 Jan 2023

HAL is a multi-disciplinary open access archive for the deposit and dissemination of scientific research documents, whether they are published or not. The documents may come from teaching and research institutions in France or abroad, or from public or private research centers.

L'archive ouverte pluridisciplinaire **HAL**, est destinée au dépôt et à la diffusion de documents scientifiques de niveau recherche, publiés ou non, émanant des établissements d'enseignement et de recherche français ou étrangers, des laboratoires publics ou privés.



Distributed under a Creative Commons Attribution 4.0 International License

Impact of past steel-making activities on lanthanides and Y (REY) fractionation and potential mobility in riverbank sediments

Christophe Hissler^{1*}, Emmanuelle Montarges-Pelletier², Hussein J. Kanbar², Mathieu Le Meur², Christophe Gauthier²

¹Luxembourg Institute of Science and Technology (LIST), Luxembourg, ²UMR7360 Laboratoire Interdisciplinaire des Environnements Continentaux (LIEC), France

Submitted to Journal:
Frontiers in Earth Science

Specialty Section:
Geochemistry

Article type:
Original Research Article

Manuscript ID:
1056919

Received on:
29 Sep 2022

Revised on:
17 Dec 2022

Journal website link:
www.frontiersin.org

Conflict of interest statement

The authors declare that the research was conducted in the absence of any commercial or financial relationships that could be construed as a potential conflict of interest

Author contribution statement

CH and EMP contributed to the conceptualization, the data curation and treatment, the designing, writing and final editing of the manuscript, the supervision and administration of the project. HJK, ML and CG participated in the draft manuscript review and final editing. EMP, HJK, ML and CG performed the core sediment sampling, the bulk sample preparation and analysis. CH performed the sequential extractions.

Keywords

Rare earth element, pollution, River sediment, Mineralogy, industrial valley

Abstract

Word count: 299

New technologies significantly disturb the natural riverine cycle of some Rare Earth Elements and Yttrium (REY). Whereas large evidence exists on the anthropogenic impact on REY dissolved and colloidal loads in rivers, there is still a knowledge gap on how suspended load could be impacted. As the river suspended matter is a key driver for the quantity of trace metal transport and mobility toward the other river compartments, it is of importance to evaluate how anthropogenic activity could affect its REY composition. Here, we report how past steel-making processes impacted the REY composition and potential mobility in riverbank sediments collected from a French River basin heavily disturbed by this industrial activity. In comparison to sediment originated from the local soil erosion, the industrial waste released in the river presented very unusual REY patterns. We observed specific LaN/GdN, LaN/LuN and Y/Ho ratios that indicate a strong heritage in the industrial waste of the iron ore used to produce steel. REY enrichments were also highlighted and can be classified as follow: Eu>Yb>Sm>Ce>Tm. The different enrichments might illustrate various fractionation processes that occurred separately on the different lanthanides inside the blast furnace according to temperature, pressure and oxygen fugacity changes. Sequential extractions performed on natural and industrial waste samples showed that REY enrichments in the industrial waste are included in one main fraction, which is strongly labile, whereas REYs contained in the sediment originating from the soil erosion are related to different mineralogical fractions having lower and more specific lability. Finally, REY composition showed that the sediment deposited on the riverbank is composed of two types of materials, which progressively evolved, after the ending of the industrial activity in this region, from a pure industrial waste in depth to a pure natural suspended sediment originated from local soil erosion at the surface.

Contribution to the field

The present study investigates REY distribution and origins in three riverbank cores of a heavily polluted river system, Northeastern France; two of those banks were proven to be full made of steel-making wastes. We examined the evolution of the REY patterns in those materials as a function of depth and hypothesize that steel-making waste presented a contrasting REY pattern due to the temperature and redox conditions inside the blast furnace during ore melting, such conditions were able to enhance fractionation between lanthanides. We also demonstrate that REY present in the blast furnace sludge might have a different mobility potential in comparison to the detrital suspended particles, originated from soil erosion. These findings may be used to assess more precisely the impact of anthropogenic activities in river systems by using REY as tracer of pollution dissemination in such aquatic ecosystems.

Funding statement

This research was funded by the Luxembourg National Research Fund (FNR) and the French National Research Agency (ANR-14-CE01-0019) in the framework of the FNR INTER ANR research program (contract no. INTER/ANR/13/9441502). The Long-Term Ecosystem Research (LTER) France, the French Water Agency Rhin-Meuse and the Region Lorraine through the research network of the Zone Atelier Moselle (ZAM) partially funded this work.

Ethics statements

Studies involving animal subjects

Generated Statement: No animal studies are presented in this manuscript.

Studies involving human subjects

Generated Statement: No human studies are presented in this manuscript.

Inclusion of identifiable human data

Generated Statement: No potentially identifiable human images or data is presented in this study.

In review

Data availability statement

Generated Statement: The datasets presented in this study can be found in online repositories. The names of the repository/repositories and accession number(s) can be found below: <https://doi.org/10.24396/ORDAR-59> and <https://doi.org/10.5281/zenodo.7447548>.

In review

Impact of past steel-making activities on lanthanides and Y (REY) fractionation and potential mobility in riverbank sediments

1 **Christophe Hissler^{1*}, Emmanuelle Montarges-Pelletier^{2,3}, Hussein J. Kanbar^{2,3}, Mathieu Le**
2 **Meur^{2,3}, Christophe Gauthier^{2,3}**

3 ¹ CAT/ENVISION/ERIN Research Group, Luxembourg Institute of Science and Technology, L-4422
4 Belvaux, Luxembourg

5 ²LIEC, CNRS, Université de Lorraine, F-54000 Nancy, France

6 ³LTSER FRANCE Zone atelier Moselle

7 *

8 Christophe
9 christophe.hissler@list.lu

Correspondence:
Hissler

10 **Keywords: rare earth elements, pollution, river sediment, mineralogy, industrial valley**

11 **Abstract**

12 New technologies significantly disturb the natural riverine cycle of some Rare Earth Elements and
13 Yttrium (REY). Whereas large evidence exists on the anthropogenic impact on REY dissolved and
14 colloidal loads in rivers, there is still a knowledge gap on how suspended load could be impacted. As
15 the river suspended matter is a key driver for the quantity of trace metal transport and mobility toward
16 the other river compartments, it is of importance to evaluate how anthropogenic activity could affect
17 its REY composition. Here, we report how past steel-making processes impacted the REY composition
18 and potential mobility in riverbank sediments collected from a French River basin heavily disturbed
19 by this industrial activity. In comparison to sediment originated from the local soil erosion, the
20 industrial waste released in the river presented very unusual REY patterns. We observed specific
21 La_N/Gd_N , La_N/Lu_N and Y/Ho ratios that indicate a strong heritage in the industrial waste of the iron ore
22 used to produce steel. REY enrichments were also highlighted and can be classified as follow:
23 $Eu > Yb > Sm > Ce > Tm$. The different enrichments might illustrate various fractionation processes that
24 occurred separately on the different lanthanides inside the blast furnace according to temperature,
25 pressure and oxygen fugacity changes. Sequential extractions performed on natural and industrial
26 waste samples showed that REY enrichments in the industrial waste are included in one main fraction,
27 which is strongly labile, whereas REYs contained in the sediment originating from the soil erosion are
28 related to different mineralogical fractions having lower and more specific lability. Finally, REY
29 composition showed that the sediment deposited on the riverbank is composed of two types of
30 materials, which progressively evolved, after the ending of the industrial activity in this region, from a
31 pure industrial waste in depth to a pure natural suspended sediment originated from local soil erosion
32 at the surface.

33 **1 Introduction**

34 Since the end of the 18th century and the technical process to eliminate the phosphorus contained in
35 the iron ore (Garcier, 2007), northern-western European countries, including the Lorraine region in
36 France, have been more active with iron and coal mining and related steel production. To ensure an

37 easy access to water source to the production facility, unforeseen changes were brought to the river
38 ecosystems, profoundly modifying the riparian landscape by physical, chemical and biological changes
39 (Picon, 2014). River water served in several steel-making processes, such as a cleaning fluid for an
40 efficient use of the blast furnace and as the receptacle of industrial wastes. Industrial wastes of many
41 different origin and composition (furnace smokes, dust and sludge from wet cleaning of furnace
42 smokes) were since then directly introduced in the river channel, transported as suspended particles or
43 stored in the riverbed (Vdović et al., 2006; Zebracki, 2008; Kanbar et al., 2017).

44 All these changes in the riverbed disturbed the natural cycle of elements, and in particular that of critical
45 elements used for the technology development. Bau and Dulski (1996) published for the first time
46 scientific evidence of an anthropogenic impact on the REY natural cycle. Since then, REY are studied
47 as emergent micropollutants because of their widespread use in industrial and medical activities (Zhang
48 et al., 2017; Knobloch et al., 2018). The various anthropogenic uses are associated with so-called REY
49 anomalies in fluvial systems worldwide (Kulaksiz and Bau, 2013). The most famous is the positive Gd
50 anomaly, related to the clinical use of Gd-based contrast agents in Magnetic Resonance Imaging (MRI),
51 which is now considered worldwide as a distinctive signature of water inputs from wastewater
52 treatment plants (Merschel et al., 2015; Parant et al., 2018; Louis et al., 2020). Until now, Gd-based
53 contrast agents are recognized as unreactive in the environment and the corresponding Gd anomaly
54 occurs only in the truly dissolved fraction, defined as the fraction passing through 10 kDa ultrafiltration
55 membranes. In most recent studies, river colloidal fractions (10 kDa – 1000 nm) were also subject of
56 REY contamination due to the effluents of a production plant for fluid catalytic cracking catalysts using
57 La and Sm (Kulaksiz and Bau, 2013; Klaver et al., 2014) or to steel making activity for Nd (Martin et
58 al., 2021). It is generally admitted that most of the REY transported by suspended particle matter,
59 (particles >1000 nm) present a natural signature like soils and bedrocks in little river systems (Hissler
60 et al., 2016). Such signature was also highlighted for larger rivers such as the Congo, Amazon,
61 Mississippi, Ohio, and Rhine rivers (Goldstein and Jacobsen, 1988; Eldefield et al., 1990; Dupré, 1996;
62 Tricca et al., 1999). Despite the discovery of anthropogenic REY in dissolved and colloidal fractions
63 of river water, only few studies observed anthropogenic impact on the REY contents of river suspended
64 particulate matter. La anomaly was observed by Klaver et al. (2014) in the Rhine River basin. Hissler
65 et al. (2015a and 2016) and Martin et al. (2021) identified a positive Ce and Nd anomalies in river
66 suspended particulate matter linked to current and historical Luxembourg steel-making activities in the
67 upper Alzette River basin. All these results strengthen how the increasing extraction and use of REY
68 is disrupting their natural biogeochemical cycles in polluted rivers. The harmful effects of REY are not
69 solely linked to the relatively recent production of technology tools, but also to historical anthropogenic
70 activities, as well as those involving steel-making. To date, the environmental risk of REY has received
71 little attention because it is perceived as relatively low in comparison to other more abundant metals.
72 Moreover, the forms in which anthropogenic REY are stored in river sediments and the processes that
73 control their mobility from sediment to the water column need to be further investigated to evaluate
74 potential biological and human health threats (Lachaux et al., 2022).

75 The present study investigates REY distribution and origins in three riverbank cores of the Orne River,
76 Northeastern France; two of those banks were proven to be full made of steel-making wastes, such as
77 blast furnace sludge (Kanbar et al., 2017; Kanbar, 2017). We examined the evolution of the REY
78 patterns in those materials as a function of depth and hypothesize that steel-making waste presented a
79 contrasting REY pattern due to the temperature and redox conditions inside the blast furnace during
80 ore melting, such conditions were able to enhance fractionation between lanthanides. We also
81 demonstrate that REY present in the blast furnace sludge might have a different mobility potential in
82 comparison to the detrital suspended particles, originated from soil erosion. These findings may be

83 used to assess more precisely the impact of anthropogenic activities in river systems by using REY as
84 tracer of pollution dissemination in such aquatic ecosystems.

85 2. Material and methods

86

87 2.1. Study site

88 From 1880 to 2008, the Lorraine region (North-East of France) had an industrial and economical
89 importance for the steel production in France and Europe. In this context, due to the local occurrence
90 of iron ore, the Orne River basin was subject to intense steel-making activity, including iron mining,
91 coke, pig iron and steel production. This industrialization severely modified the physics and chemistry
92 of the Orne River and its major riverbed. The reminiscent impact of this past industry on the Orne
93 River geomorphology, banks and water quality were also already referenced in several studies
94 (Abuhelou, 2016; Kanbar et al, 2017; Losson et al., 2020; Martinez-Carreras et al., 2021). In the
95 beginning of the steel-making industry and during almost the whole period of this activity, tons of blast
96 furnace sludge and other fine particle suspensions were daily discharged in the Orne River, provoking
97 lateral floods due to the filling of the main river course. The amount of suspended particles introduced
98 in the river was estimated to be 31t per day in 1972. Dredging was lately operated in the 60's and 80's,
99 leaving contaminated banks for several kilometers. In the last period of the steel-making activity, to
100 guarantee sufficient water resource for the cooling of furnaces, two dams were built (1960 for
101 Moyeuve Grande dam and 1973 for Homecourt dam). Those dams, following the European water
102 rules, were recently opened, showing up the banks made of industrial wastes.

103 The Orne River joins the Moselle River and belongs to the Rhine River basin. This river flows in the
104 northeastern France, is 90 km long from its source in Ornes to the confluence with the Moselle River
105 in Richemont and has a basin area of 1,268 km² (Fig. 1). The geology of the Orne River basin can be
106 divided into two main parts, (i) a clayey depression in the Woëvre region made of easily eroded soft
107 Lias marl lithologies and (ii) a calcareous plateau at the Pays-Haut, starting in Jarny and belonging to
108 middle Jurassic lithologies, an Aalenian calcareous sandstone and some Bajocian limestones. The
109 Aalenian calcareous sandstone is a ferriferous formation used as iron ore in this region. It is made of
110 an oolitic ferriarenite that includes more than 10 layers, each layer being several meters thick.

111

112 Figure 1: The Orne River basin, the downstream area where steel-making facilities and dams were
113 installed and a focus on the influence zone (orange dashed line) of the Moyeuve dam, also called Beth
114 dam with the location and the log description of the three riverbank cores selected in this study (from
115 upstream to downstream: JOSAN, JOEP and BETHUP).

116

117 2.2. Sampling and sample preparation

118 The cores were sampled at three distinct places, all located in the influence zone of the Beth dam (figure
119 1). This dam was operating from 1960 to 2019 providing a water reservoir for blast furnace cooling
120 between 1960 and 1980. The most upstream site, JOSAN, is located in the beginning of the influence
121 zone, on the right side of the river. The bank was cored in 2015 using a 9 cm tube diameter from a
122 floating platform (Quadriraft from GEHCO laboratories, Tours University, France). The core was 51.5
123 cm long. The second core site, JOEP is located in the very end of the first division of Jœuf steel-making
124 site. This zone was dredged in 1988, the riverbanks are not natural, and the flowing waters incised the
125 riverbed. The bank was cored in 2017 using a piston corer (diameter 6 cm). The core was 82 cm long.
126 The last core (BETHUP) was sampled downstream on the right bank few dozen meters before the Beth

127 dam (Kanbar et al 2017) in 2014. The core was 131 cm long. The location and characteristics of the
128 three cores are provided in Figure 1.

129 After coring, the tubes were filled with flower foam to minimize the air volumes and were hermetically
130 closed with plastic caps and thick tape. Back to the laboratory, the cores were cut lengthwise, and one
131 half was immediately stored in a glove bag with N₂ gas flow to prevent oxidation. After deep
132 examination of the core physical aspects, texture and color, 2 to 3 cm slices were cut. The different
133 slices were weighed, frozen at -18 °C and freeze-dried. The final amount of freeze-dried sediments was
134 weighed and water content was calculated. For each slice, 1.5 g aliquot was sampled after soft
135 homogenization, and was ground. The ground samples were used for element analysis.

136 A sequential leaching extraction was performed on aliquots of two freeze-dried samples from JOSAN
137 and JOEP cores; they represent the recent deposition at the surface of the riverbed and the historical
138 steel waste that can be found at the bottom of the core sediments, respectively. The used procedure
139 (Hissler et al., 2015b), adapted from Steinmann and Stille (1997), allows to identify the mobile and
140 labile part of the sediment and to recover the leachable fractions, which are considered to represent
141 adsorbed elements and those fixed in acid-soluble phases. With this technique, we assume that the
142 residual fraction and the different leachable fractions are operationally defined because of the existing
143 continuum between residual and leachable phases (Stille and Clauer, 1994). Sequential leaching was
144 performed in four steps using demineralized MilliQ water (Millipore system – L1 leachate), acetic acid
145 (0.05N Hac – L2 leachate), hydrochloric acid (1N HCl – L3 leachate) and nitric acid (2N HNO₃ – L4
146 leachate). All these reagents are of ultrapure quality and the measured blanks were always below the
147 detection limit.

148

149 2.3. REY and related major element analysis

150 Major (Na, Mg, K, Ca, Al, Mn, Fe, Si and P) and REY (La, Ce, Pr, Nd, Sm, Eu, Gd, Tb, Dy, Ho, Er,
151 Tm, Yb, Lu and Y) were detected in the bulk sediments, the bedrocks and in the leaching residual
152 sediment fractions by inductively coupled plasma optical emission spectrometry (ICP-OES) and
153 inductively coupled plasma mass spectrometry (ICP-MS), respectively. These analyses were
154 performed at SARM (Service d'Analyse des Roches et des Minéraux – CRPG, Vandoeuvre-lès-Nancy,
155 France) and all analytical methods were subject to QC/QA procedures using certified reference
156 materials (Carignan et al., 2001). The associated results can be found on the ORDAR data repository
157 (<https://doi.org/10.24396/ORDAR-59>).

158 The major and trace elements concentrations of the leachates were determined using ICP-MS (Agilent
159 7900) associated with an ISIS 3 (Agilent) injection system at LIST. Analyses were conducted in He
160 mode and ¹⁰³Rh and ¹⁸⁵Re were used as internal standards. Analytical blank values were less than 1%
161 of the lowest sample concentrations for all elements. For all REY, the detection limit was 0.3 ng L⁻¹
162 and the quantification limit was 1.0 ng L⁻¹. Calibration standards were prepared with Multi elements
163 ICP standard solutions (CHEM-LAB Analytical) diluted in 1% HNO₃. We calculated the mass balance
164 during the complete sequential extraction for each analyzed element and we compared the total
165 concentrations obtained by sequential extraction (L1+L2+L3+L4+residu) to that obtained on the bulk
166 sample. For a given element, the two total concentrations presented differences but were significantly
167 correlated for both major and REY elements with R² of 0.99 for JOSAN and JOEP, illustrating that the
168 differences are consistent between most of the elements for the two samples, only Ca presented more
169 contrasted results. JOSAN had close total concentrations between the two methods, whereas sequential
170 extraction on JOEP showed higher total concentrations for most of the elements. This could be
171 attributed to heterogeneities in the two JOEP aliquots used for both methods. The associated results
172 can be found on a Zenodo data repository (<https://doi.org/10.5281/zenodo.7447548>).

173 2.4. Mineralogy

174 X-ray diffraction (XRD) analyses were performed at LIEC laboratory on the bulk ground sediment
 175 layers to determine the major crystalline phases. A D8 Advance Bruker diffractometer with a Co K_{α1}
 176 radiation source, operated at 35 kV and 45 mA ($\lambda = 1.7902 \text{ \AA}$), was used. XRD patterns were collected
 177 on the angular range (2θ) of $3 - 64^\circ$, with a 0.034° step size and a 3 sec collecting time. All layers were
 178 subjected to XRD analyses, and for clearness purpose, only relevant patterns are presented.

179

180 2.5. REY anomaly calculations

181 The unusual REY patterns that were observed in the studied samples make the quantification of the
 182 relative REY anomalies difficult. For this reason, we assumed that some REY elements are not
 183 impacted during the described processes and can be used as reference element to calculate anomalies
 184 for the impacted elements during the melting process of the steel production. This important issue is
 185 also discussed more in detail in §4.2.

186 The calculation of the REY anomalies are given below:

187

$$188 \quad Ce/Ce^* = Ce / (\frac{1}{2}La + \frac{1}{2}Pr) \quad \text{eq. 1}$$

$$189 \quad Sm/Sm^* = Sm / (\frac{2}{3}Nd + \frac{1}{3}Gd) \quad \text{eq. 2}$$

$$190 \quad Tm/Tm^* = Tm / (\frac{2}{3}Er + \frac{1}{3}Lu) \quad \text{eq. 3}$$

$$191 \quad Yb/Yb^* = Yb / (\frac{1}{3}Er + \frac{2}{3}Lu) \quad \text{eq. 4}$$

192

193 **3. Results**

194

195 3.1. mineralogy, major element contents and distributions along the core profiles

196 JOSAN sediments display a detrital X-ray diffraction pattern, predominated by clay minerals, quartz
 197 and feldspars as silicates, and by calcite as carbonates (Fig. 2a). JOSAN core was described as a series
 198 of silt, clay layers and leaf layers (Kanbar, 2017; De la Cruz Barrón et al., 2018). The clay minerals
 199 are mainly constituted of illite, interlayered illite/smectite and chlorite. In a previous publication (De
 200 la Cruz Barrón et al., 2018), we could evidence the similarity between clay mineralogy of the Orne
 201 River suspended particulate matter and the surface sediments sampled in JOSAN. With depth, the
 202 mineralogy of JOSAN does not show strong modifications, the apparent amount of quartz and calcite
 203 follows the particle size distribution and the organic matter content.

204 The mineralogy of BETHUP core was previously described (Kanbar et al., 2017). Below surface
 205 sediments that display a detrital mineralogical fingerprint like that of JOSAN samples (quartz, calcite,
 206 feldspars, and clay minerals), steel-making wastes can already be observed. This is proven by iron
 207 bearing phases, oxides and (hydr)oxides, ferrous and ferric, crystalline and non-crystalline phases. The
 208 iron phases are assigned to dust particles from the blast furnaces (wustite FeO, magnetite Fe₃O₄), to
 209 pristine iron ore (goethite FeOOH) and to weathering products (Fe-clays). The relatively low intensity
 210 of quartz diffraction lines and the presence of iron oxide diffraction lines in the 38-45 2θ region are
 211 the main characteristics of the XRD patterns of those steel-making wastes (Fig. 2a, curves 4 and 5).
 212 JOEP material displays similar mineralogy to BETHUP deposit with a relatively lower content of iron

213 crystalline phases (wustite, magnetite), but displaying goethite, the main iron phase of the iron ore
 214 (Dagallier et al., 2002, Kanbar et al., 2017). Goethite particles in BETHUP and JOEP materials are
 215 shown to be similar in shape, crystallinity and composition to the goethite of iron ore, which is the
 216 Aalenian calcareous sandstone (Kanbar et al., 2017). JOEP material appears relatively enriched in
 217 calcite (Fig. 2b). The origin of such high amount of calcium carbonates was assumed to be related to
 218 the regular inputs of lime in the river (Garcier et al 2007), also evidenced by thin white layers (Fig.
 219 2c). Beside industrial borne minerals, JOEP and BETHUP cores still display a low contribution of
 220 detrital materials (Fig. 2a, curves 4 and 5).

221

222 Figure 2: a. XRD patterns for JOSAN, JOEP and BETHUP samples. The three top curves correspond
 223 to surface sediments at the three river stations from upstream to downstream: 1: JOSAN surface
 224 sediment; 2: JOEP surface sediment; 3: BETHUP surface sediment. The two bottom curves represent
 225 deep layers of JOEP (4) and BETHUP (5) cores. Abbreviations of mineral phases: quartz (Q); calcite
 226 (C); Feldspars (F); clay minerals (CM); magnetite (M); goethite (G); wustite (W); Fe-clays (FeC).

227 b. zoom on calcite diffraction lines for deep samples at JOEP (4) and BETHUP (5).

228 c. observation of the thin white calcium layers at JOEP

229

230 The evolution of the major element contents in the bulk BETHUP samples show three groups (Fig.
 231 3a). Si, Na, Al, K and Ti contents progressively decrease with depth and present strong linear
 232 correlations (Kanbar et al., 2017). On the contrary, elements of the second group, Fe, Mn and P have
 233 a content progressively increasing with depth and present strong linear anti-correlations with Si and
 234 other alkaline elements. The last group corresponds to Mg and Ca contents that do not present any
 235 significant evolution trend with depth. Ca profile is partly related to the input of lime sludge in the river
 236 during the industrial activity. A very similar vertical evolution with depth is also observed for the core
 237 collected at JOEP and similar groups can be defined (Fig. 3b). The major element contents measured
 238 in the core collected at JOSAN present different results (Fig. 3c). Si and Fe are close to the values
 239 found in the Group I, whereas Ca is higher and increases with depth.

240

241 3.2. REY patterns and content in the local lithologies and the bulk core layers

242 REY contents are in the same order of magnitude for the three main lithologies that cover the studied
 243 river basin (Fig. 4a). By normalizing to the Post-Archean Australian Shale (PAAS, Taylor and
 244 McLennan, 1985), they show very distinct types of distribution patterns (Fig. 4a). While the Toarcian
 245 marls have a flat pattern with a slight middle REY (from Sm to Tb) enrichment, shown by Eu/Eu^*
 246 anomaly of 1.2, the Bajocian limestone present a strong Ce negative anomaly ($Ce/Ce^*=0.5$) and is
 247 depleted in heavy REY (from Dy to Lu) with $La_N/Lu_N=2.1$. Both lithologies display larger Y/Ho ratios
 248 of 32 and 105, respectively. The Aalenian calcareous sandstone, which includes the iron ore used for
 249 the steel production in this area, has a PAAS-normalized REY pattern characterized by a large
 250 depletion in light REY (from La to Nd), with $La_N/Lu_N=0.4$, and a lower Y/Ho ratio of 24.

251 The REY contents of surface sediments lie in the same range as those of the lithologies. However, a
 252 decrease can be observed down the cores for JOEP and BETHUP. From the surface to the bottom of
 253 the BETHUP (Fig. 4b) and JOEP (Fig. 4c) cores, the REY patterns can be separated in four groups
 254 according to the Si and Fe contents (Kanbar et al., 2017). At JOSAN, only two different groups can be
 255 distinguished (Fig. 4d). The calculated PAAS-normalized patterns evolve coherently between the
 256 groups with the SiO_2 content at the three locations. Close to the surface, the patterns are flat (average

257 $La_N/Lu_N=1.0$) with a little middle REY enrichment (average $Eu/Eu^*=1.1$) (Fig. 4bcd). In the bottom
 258 layers of the BETHUP and JOEP cores, the PAAS-normalized REY patterns look very unusual
 259 according to what is known in Earth Critical Zone environments (Fig. 4bc). The main characteristics
 260 of these patterns are a light REY depletion (average $La_N/Lu_N=0.5$) and multiple enrichments in several
 261 lanthanides that can be characterized by the related anomalies: Ce/Ce^* (1.1), Sm/Sm^* (1.5), Eu/Eu^*
 262 (1.7), Tm/Tm^* (1.2) and Yb/Yb^* (1.4) (Fig. 4bc). The REY pattern of the samples located between the
 263 surface and the deepest layer present a coherent and regular evolution with depth in between these two
 264 samples, as illustrated by the Y/Ho ratio evolution with depth at BETHUP (Fig. 3a).

265

266 **Figure 3:** Evolution with depth of Si, Fe and Ca contents, as atomic percentage, and the REY pattern
 267 characteristics observed in the core collected from the Orne Riverbank at (a) BETHUP, (b) JOEP and
 268 (c) JOSAN sampling locations. REY anomalies and ratios are calculated using the Aalenian calcareous
 269 sandstone-normalized patterns.

270

271 **Figure 4:** PAAS-normalized REY patterns of bedrocks covering the Orne River basin (a) and of the
 272 three selected riverbank cores normalized by the SiO_2 content (b: BETHUP, c: JOEP, d: JOSAN). The
 273 groups are defined according to Kanbar et al. (2017).

274

275 3.3. REY patterns, concentrations and major element concentrations in the leachates and residual 276 fractions

277 The REY concentrations in the leachates of the first two steps of the sequential extraction (water and
 278 0.05N Hac) were negligible and most often below the detection limits. Therefore, only the results
 279 related to the two last leaching steps, using 1N HCl (L3) and 2N HNO_3 (L4), and the residual (R)
 280 fractions are reported. The samples from the surface and the deepest layers have very contrasting
 281 results.

282 At the surface, in JOSAN sample, the leaching yield ranged between 20% for Lu and 41% for Eu and
 283 Gd (Fig. 5a). This indicates that the middle REY were the most leached during the entire extraction
 284 procedure. REY were more concentrated in HCl compared to HNO_3 leachates. The PAAS-normalized
 285 REY patterns related to these last two extraction steps have differences in their Eu/Eu^* , La_N/Lu_N and
 286 Y/Ho ratios. HCl leachates present higher La_N/Lu_N (1.5 vs. 1.1) and Y/Ho (33 vs. 23) ratios than HNO_3 ,
 287 whereas HNO_3 leachates have higher Eu/Eu^* (1.3 vs. 1.1) (Fig. 5a). As a result, the pattern of the
 288 residual fraction is flat, illustrating that most of the mineral fractions that contributed to this middle
 289 REY enrichment were leached during the sequential extraction process and that, according to PAAS,
 290 the residue presents lower REY concentrations but similar REY distribution.

291 In the JOEP sample, the leaching yield ranged from 78% for Lu and more than 90% for Eu and the
 292 heavy REY were the less leached (Fig.5b). In comparison to the previous sample at JOSAN, the PAAS-
 293 normalized patterns of the two leachates are similar with HCl leachate being about two times more
 294 concentrated. They look like very similar to the pattern of the bulk sediment sample described
 295 previously (Fig. 4bc). As a consequence, the PAAS-normalized pattern of the residual fraction is
 296 strongly depleted in light and medium REY and present the lowest La_N/Lu_N ratio measured for all
 297 samples (0.2).

298

299 **Figure 5:** Contribution of leachates L3 and L4 (blue vertical bars) and residual R (grey vertical bars)
 300 fractions and related PAAS-normalized REY patterns (lines) in (a) the Group I (at JOSAN) and (b)

301 Group IV (at JOEP). White circles correspond to the bulk sample before leaching whereas the green,
 302 the orange and the dark grey represent the 1N HCl (L3), 2N HNO₃ (L4) and residual (R) fractions,
 303 respectively.

304

305 The sequential extractions performed for the major elements on the two selected samples corroborate
 306 most of the REY results. In the JOSAN sample, Na, Mg, K, Al and Fe are mainly contained in the
 307 residual fraction and present extraction yields below 20% (Fig. 6a), whereas Ca (98%), Mn (63%) and
 308 P (32%) are more labile and mainly present after L2 and L3 for Ca and after L3 and L4 for Mn and P.
 309 The partitioning of Ca, Mn and P between the different leachates of JOEP sample and the respective
 310 extraction yields are very similar to JOSAN (Fig. 6b). However, P is distributed among less labile
 311 fractions in JOEP and mainly present in L4 leachates. All the other elements, except K, present larger
 312 extraction yields in comparison to JOSAN, from 28% for Fe to 74% for Na.

313

314 Figure 6: Extraction yield and contribution of leachates (blue vertical bars) and residual (grey bars)
 315 fractions of total REY and related major element concentrations in the Group I at JOSAN (a) and Group
 316 IV at JOEP (b). Leachate with MilliQ water (L1); leachate with 0.05N Hac (L2), leachate with 1N HCl
 317 (L3); leachate with 2N HNO₃ (L4); residual fraction (R).

318

319 4. Discussion

320

321 4.1. Lithological heritage on the REY pattern of the core surface layer (Group I)

322 The REY normalized patterns of the surface sediments present strong similarities with the Toarcian
 323 marls that cover about 70% of the basin area (Fig. 1). Both bedrock and surface sediment samples have,
 324 according to PAAS, La_N/Lu_N ratios about 1 and slight upward convexities for the middle REY (MREY)
 325 explained by Eu/Eu* about 1.2 (Fig. 3 and 4). One of the main differences is the Y content that is
 326 depleted in the surface sediments, with a Y/Ho ratio about 27, when Y/Ho ratio is 32 in the lithology.
 327 The MREY enrichments are also like those of suspended sediments transported larger world rivers as
 328 the Congo, Amazon, Mississippi, Ohio, and Rhine Rivers (Goldstein and Jacobsen, 1988; Elderfield et
 329 al., 1990; Dupré et al., 1996; Tricca et al., 1999; Klaver et al., 2014). This enrichment might be related
 330 to the presence of phosphate minerals because many phosphatic minerals of not only biogenic,
 331 authigenic and diagenetic origins, but also magmatic origins show this upward convexity (Hannigan
 332 and Sholkovitz, 2001; Stille et al., 2009). As already shown by Hissler et al. (2016) and more recently
 333 by Martin et al. (2021) in the neighbouring Alzette River basin in Luxembourg, the soils surrounding
 334 this latter area display P- and REY-bearing mineral phases that can characterize similar weak MREY
 335 enrichments. The geology that constitutes the Orne River and the upper Alzette River are the same and
 336 we expect similar mineral contribution and related REY pattern of the suspended particles originated
 337 from the soil erosion in the Orne watershed.

338 This assumption is also strengthened by the results obtained with the sequential extraction performed
 339 on the JOSAN sample. The mineral fractions related to the MREY enrichment were completely leached
 340 after the entire extraction procedure (Fig. 5a). MREY extraction yield were the highest, between 38
 341 and 41% of the total REY content. As a result, the MREY enrichment disappeared in the PAAS-
 342 normalized pattern of the residual fraction no with Eu/Eu* = 1.1. The L3 and L4 leachates do not show
 343 similar PAAS-normalized REY distribution patterns. Most enriched in REY is L3 with a MREY and
 344 Y enrichments and a HREY depletion. L4 is characterized by MREY enrichment and LREY, HREY

345 and Y depletions. Based on these results, we can state that L3 and L4 leachates represent two distinct
346 phases of minerals that are progressively leached from pH=3.0 (L3) to pH<1.0 (L4); these conditions
347 could dissolve MREY-bearing phosphate, like apatite, monazite, xenotime or rhabdophane minerals
348 (Hissler et al., 2015b). Indeed, the LREY depletion accompanied with the MREY enrichment in L4 is
349 typical to the apatite REY pattern, as observed by Aubert et al. (2001). Additionally, most of the
350 phosphorous (22%) was leached during L4 extraction step (Fig. 6a). Therefore, the REY composition
351 of the surface sediment collected at the three locations originate from the erosion of the surrounding
352 and upstream soils. They have been progressively transported from their source, in the upstream
353 agricultural part of the basin, to the Orne River during successive flood events. Our results may also
354 show that during fluvial transport of the soil particles, Y could be preferentially leached in comparison
355 to Ho, as seen in Fig. 4.

356

357 4.2. Origin of the REY pattern found in deep core layers.

358 Very different is the PAAS-normalized REY pattern of the steel production wastes that constitute the
359 deeper layers of the JOEP and BETHUP cores. As shown in Fig. 3 and 4, their REY distribution is
360 unusual in comparison to lithological pattern from Group I found for the surface layers of the three
361 cores. Two main characteristics can define the different pattern of Group IV samples.

362 The first characteristic is the important depletion of LREY compared to MREY and HREY and coupled
363 with a Y depletion. These depletions are represented by La_N/Lu_N , La_N/Gd_N ratios ranging from 0.40 to
364 0.50 and a Y/Ho ratio about 25 (Fig. 4). These characteristics are very close to the ratios that
365 characterize the Aalenian calcareous sandstone (Fig. 7), which was used as iron ore for the local steel
366 production in the Orne River valley (Kanbar et al., 2017). This latter presents La_N/Lu_N , La_N/Gd_N and
367 Y/Ho ratios of 0.40, 0.40 and 24, respectively. We assume here that these two characteristic depletions
368 originate from the initial REY signature of the iron ore and that these REY characteristics were
369 preserved during the melting process inside the blast furnaces or converters of steel-making facilities.

370

371 Figure 7: Aalenian calcareous sandstone-normalized REY patterns for the 16 riverbank samples of
372 group IV at JOEP and BETHUP. The black line corresponds to the average value and the light grey
373 area to the standard deviation (n=16).

374

375 The second characteristic is the enrichments in Ce, Sm, Eu, Tm and Yb in comparison to the surface
376 layers (Fig. 4). All these enrichments present good level of correlations and by comparing them using
377 single linear regression (Fig. 8), different regression slopes allow to group these five anomalies
378 according to the 1:1 line. This statistical analysis suggests that especially Eu and Yb anomalies, but
379 also Sm anomaly, behave more similarly than Ce and Tb anomalies. For this Group IV, we expected
380 that the sequential extraction would reveal different chemical status for the REY anomalies. However,
381 for JOEP samples, the amounts of chemically extracted REYs are closer to the total contents. The
382 leaching yields range from 61 to 79% for the HREY, 80 to 87% for the MREY and 81 to 84% for the
383 LREY (Fig. 5b). Interestingly, all REY anomalies previously identified in bulk samples are preserved
384 in L3 and L4 leachates (Fig. 5b). Even the residual fractions have some remnant of the leached patterns.
385 The used sequential leaching was not able to separate the different REY enrichments observed
386 according to the supposed chemical status. For this group IV, the sequential extraction suggests that
387 all observed REY enrichments may belong to same material phases formed during the melting/cooling
388 processes of the pig iron and steel production.

389 Concerning the major elements, it appears that K, Al and Fe present the lowest leaching yields during
 390 the complete procedure (<50% of the total contents), and significantly lower than the yields for REY.
 391 These latter present closer results with Al, Mn and P (Fig. 6b), having respective leaching yield of 50,
 392 73 and 54%. The similar leaching yields of Al, Mn, P and REY (L3 and L4) support that REY leached
 393 from JOEP are linked to Al, Mn and P phases that formed in the blast furnace during steel production.
 394 However, as the mineralogy analysis demonstrated the presence of numerous iron oxides, we might
 395 also take into account that only a fraction of iron bearing phases was efficiently leached).

396 The fractionation of the different lanthanides was certainly controlled by processes that can target
 397 lanthanides having very distinct physical properties and distributed over the entire REY spectra from
 398 LREY to HREY. Temperature (up to 1200-1300 °C) and oxygen conditions within the blast furnaces
 399 have certainly induced this partitioning. As experimented by Ingrao et al. (2019), the positive Eu/Eu*,
 400 Yb/Yb* and Sm/Sm* anomalies observed in this study can be attributed to the preferential incorporation
 401 of these elements in their divalent state in the furnace fumes. Reductive conditions can be at the origin
 402 of these anomalies by enhancing the formation of divalent species Eu²⁺, Yb²⁺ and Sm²⁺. Previous
 403 studies also suggested that in such conditions, only one phase seems controlling the REY budget and
 404 that Eu and Yb anomalies are attributed to preferential evaporation and condensation of the REY
 405 (Lodders, 1996; Dickinson and McCoy 1997).

406 However, Ce and Tm enrichments might have different explanations. Indeed, Ce naturally occurs in
 407 two different valence states according to redox conditions Ce^{III} to Ce^{IV}. The positive anomaly of Ce
 408 can only form during specific oxidative conditions, as this oxidation to Ce^{IV} is combined with the
 409 formation of CeO₂ and enhances the adsorption of Ce on mineral phases (Braun et al., 1990). The
 410 process leading to the Ce anomaly could be related to the latest stage of the waste material production
 411 when oxidative conditions took place during the cooling or wet cleaning of fumes. Supplementary
 412 analyses are necessary, such as the investigation of Ce^{IV}/Ce^{III} ratio.

413

414 Figure 8: Relationship between Eu/Eu* and related REY anomalies calculated for the core
 415 riverbank samples at BETHUP location. The color refers to the group of REY defined in Fig. 4.

416

417 4.3. Natural sediment vs. steel industry waste: a two end-member mixing in the riverbank system

418 Figures 3 and 4 show how the different REY pattern characteristics progressively evolve in between
 419 two end-members: (i) the surface layer of the riverbank cores, also identified as Group I at BETHUP
 420 sampling site, and (ii) the bottom layers corresponding to the industrial waste released in the river and
 421 referred to as Group IV. La_N/Lu_N and Y/Ho regularly decrease and the Eu, Yb, Sm, Ce and Tb
 422 enrichments regularly increase from Group I to Group IV. We also show that Group I and Group IV
 423 REY properties present very strong similarity with bedrocks, Toarcian marl and Aalenian calcareous
 424 sandstone, respectively. If we plot the different core samples and the two latter lithologies in a La_N/Lu_N
 425 vs. ΣREY/SiO₂ diagram, the riverbank layers at JOEP and BETHUP are distributed along a mixing
 426 curve between the Toarcian marls and the Aalenian sandstone (Fig.9).

427 For JOSAN core, we could not detect the presence of the industrial steel-making waste, the La_N/Lu_N
 428 remains stable about 0.8, and the core samples are out of the line between the two extremes Toarcian
 429 marl and Aalenian sandstone. Interestingly, the surface layers of the three cores present very similar
 430 La_N/Lu_N vs. ΣREY/SiO₂ values (Fig. 9).

431 This graph indicates that the intermediate layers of JOEP and BETHUP cores contain REY bearing
 432 phases from the soil erosion and from the steel-making activity. Detrital contribution was also

433 suggested in these deep core layers by the presence of quartz (XRD) and clay minerals (TEM analyses,
434 Kanbar et al . 2017). From the beginning of steel production until the complete ending of the industrial
435 activity, the industrial waste release was not constant, and due to environmental regulation in the 70s
436 (Garcier al 2007) the volumes of industrial particles rejected to the river were significantly reduced.
437 The distribution of REY in Group IV samples of JOEP and BETHUP cores may also highlight the
438 different man induced activities performed in the vicinity of these two coring stations (quantity released
439 in the riverbed, liming of industrial waste, different dredging events), as well as natural processes
440 affecting the bank morphology (bioturbation, riverbank erosion/deposition during floods). Indeed, the
441 material stored in BETHUP might display a sequence including the dredging period in the late 80's.
442 JOEP banks display clear interlayers of lime sludge (fig. 2c) and is far more depleted in detrital
443 minerals, with almost no Quartz detected from the XRD pattern (Fig. 2a). However, the little
444 information that still exists on the history of this industrial valleys does not allow to reconstruct the
445 precise chronology of the different sampling sites. However, the information gained in this study are
446 of interest to quantify industrial waste contribution in the suspended sediment transported in the Orne
447 River, especially after the opening of the dams that will generate higher erosion in the riverbed and
448 increase the transport of REY polluted particles to the Orne River and downstream in the Moselle
449 River.

450

451 Figure 9: Relationship between the sum of REY concentrations normalized by SiO₂ concentration and
452 the PAAS-normalized La_N/Lu_N ratio for the riverbed sediment samples, the Toarcian marl and the
453 Aalenian calcareous sandstone collected in the Orne River basin. Also are indicated on the mixing line
454 the contribution, in %, of the industrial waste in the bulk core sediment samples. The color refers to
455 the group of REY defined in Fig. 4.

456

457 5. Conclusion

458 Whereas the anthropogenic impact on colloidal and dissolved REY transported in rivers is now well
459 established worldwide, there is still only few studies that detected any effect of human activity on
460 suspended and riverbed sediments. This new contribution presents for the first time a direct and clear
461 effect of an industrial process on the REY composition in riverbank sediments and on its temporal
462 evolution after the decline of the industry.

463 The unusual REY patterns that were observed in the sediment of the Orne River are directly related to
464 the past steel-making activity. The processes involved during the production of steel gave to the studied
465 industrial waste a specific REY signature constituted by a heavy REY enrichment, originated from the
466 used iron ore, and specific Ce, Sm, Eu, Tm and Yb enrichments. The fractionation that happened
467 between these latter elements and the other lanthanides is certainly due to two processes. On the one
468 hand, the reduction of the usual trivalent form to Eu²⁺, Yb²⁺ and Sm²⁺ in the temperature and oxygen
469 conditions inside the blast furnace. On the other hand, the oxidative conditions that took place during
470 the waste material cooling may favour the precipitation and adsorption of Ce.

471 We also show that the REY trapped in the industrial waste, at the bottom of the riverbank sediments,
472 is more labile than the REY transported on natural particles coming from soil erosion. They may
473 present a higher potential to be mobilized from sediment particles to the water column. This is now a
474 crucial issue in this river basin because of the opening of the dams that will increase the erosion of
475 these contaminated sediments. However, the specific REY pattern that characterize them is a useful
476 information to trace their fate and to evaluate potential biological and human health threats.

477

478 6. Supplementary material and data availability

479 The data used in this study are publicly available on ORDAR data repository for the total element
480 content of all core samples (<https://doi.org/10.24396/ORDAR-59>) and on a Zenodo data repository for
481 the sequential leaching analyses (<https://doi.org/10.5281/zenodo.7447548>).

482

483 7. References

484 Abuhelou, F., (2016). Spatial and temporal variations of the occurrence and distribution of polycyclic
485 aromatic compounds in a river system affected by past industrial activities. PhD dissertation, Université
486 de Lorraine, France.

487 Aubert, D., Stille, P., Probst, A. (2001). REE fractionation during granite alteration, soil formation,
488 migration and removal by dissolved and suspended loads from small river systems in the Vosges
489 mountains: chemical and Sr-Nd isotopic evidence. *Geochim. Cosmochim. Acta* 65 (3), 387–406.
490 doi:10.1016/S0016-7037(00)00546-9

491 Bau, M., Dulski, P. (1996). Anthropogenic origin of positive gadolinium anomalies in river waters.
492 *Earth Planet. Sci. Lett.* 143, 245–255. doi: 10.1016/0012-821X(96)00127-6

493 Braun, J.-J., Pagel, M., Muller, J.P., Bilong, P., Michard, A., Guillet, B. (1990). Cerium anomalies in
494 lateritic profiles. *Geochim. Cosmochim. Acta* 54, 781–795. Doi: 10.1016/0016-7037(90)90373-S

495 Carignan, J., Hild, P., Mevelle, G., Morel, J., Yeghicheyan, D. (2001). Routine analyses of trace
496 elements in geological samples using flow injection and low pressure on-line liquid chromatography
497 coupled to ICP-MS: a study of geochemical reference materials BR, DR-N, UB-N, AN-G and GH.
498 *Geostand. Geoanal. Res.* 25, 187–198. doi: 10.1111/j.1751-908X.2001.tb00595.x

499 Dagallier, G., Grgic, D., Homand, F. (2002). Caractérisation minéralogique et microtexturale du
500 vieillissement anthropique du minerai de fer lorrain. *CRGeosci.* 334, 455–462. doi:10.1016/S1631-
501 0713(02)01783-2

502 De la Cruz Barrón M, Merlin C, Guilloteau H, Montargès-Pelletier E and Bellanger X (2018).
503 Suspended Materials in River Waters Differentially Enrich Class 1 Integron- and IncP-1 Plasmid-
504 Carrying Bacteria in Sediments. *Front. Microbiol.* 9:1443. doi: 10.3389/fmicb.2018.01443

505 Dickinson, T. L., McCoy, T. (1997). Experimental rare-earth element partitioning in oldhamite:
506 Implications for the igneous origin of aubritic oldhamite. *Meteorit. Planet. Sci.* 32, 395–412. doi:
507 10.1111/j.1945-5100.1997.tb01283.x

508 Dupré, B., Gaillardet, J., Rousseau, D., Allègre, C.J. (1996). Major and trace elements of riverborne
509 material: the Congo Basin. *Geochim. Cosmochim. Acta* 60 (8), 1301–1321. doi: 10.1016/0016-
510 7037(96)00043-9

511 Elderfield, H., Upstill-Goddard, R., Sholkovitz, E.R. (1990). The rare earth elements in rivers,
512 estuaries, and coastal seas and their significance to the composition of ocean waters. *Geochim.*
513 *Cosmochim. Acta* 54 (4), 971–991. Doi: 10.1016/0016-7037(90) 90432-K.

- 514 Garcier, R.J. (2007). Rivers we can't bring ourselves to clean – historical insights into the pollution of
515 the Moselle River (France), 1850–2000. *Hydrol. Earth Syst. Sci.* 11: 1731–1745. doi: 10.5194/hess-
516 11-1731-2007
- 517 Goldstein, S. J.; Jacobsen, S. B (1988). Nd and Sr isotopic systematics of river water suspended
518 material: implications for crustal evolution. *Earth Planet. Sci. Lett.* 1988, 87, 249–265. doi:
519 10.1016/0012-821X(88)90013-1
- 520 Hannigan, R.E., Sholkovitz, E.R. (2001). The development of middle rare earth element enrichments
521 in freshwaters: weathering of phosphate minerals. *Chem. Geol.* 175, 495-508. doi: 10.1016/S0009-
522 2541(00)00355-7
- 523 Hissler, C., Stille, P., Iffly, J.F., Guignard, C., Chabaux, F., Pfister, L. (2016). Origin and Dynamics of
524 Rare Earth Elements during flood events in contaminated river basins: Sr-Nd-Pb evidence. *Environ.*
525 *Sci. Technol.* 50, 4624-4631. doi: 10.1021/acs.est.5b03660
- 526 Hissler, C., Hostache, R., Iffly, J.F., Pfister, L., Stille, P. (2015a) Anthropogenic rare earth element
527 fluxes into floodplains: coupling between geochemical monitoring and hydrodynamic-sediment
528 transport modelling. *CRGeosci.* 347, 294–303. doi: 10.1016/j.crte.2015.01.003
- 529 Hissler, C., Stille, P., Juilleret, J., Iffly, J.F., Perrone, T., Morvan, G. (2015b). Elucidating the formation
530 of terra fusca using Sr-Nd-Pb isotopes and rare earth elements. *Appl. Geochem.* 54, 85-99. doi:
531 10.1016/j.apgeochem.2015.01.011
- 532 Ingrao, N.J., Hammouda, T., Boyet, M., Gaborieau M., Moine B.N., Vlastelic, I., Bouhifd, M.A.,
533 Devida J.-L., Mathon, O., Testemale D. (2019). Rare earth element partitioning between sulphides and
534 melt: Evidence for Yb²⁺ and Sm²⁺ in EH chondrites. *Geochim. Cosmochim. Acta* 265, 182–197. doi:
535 10.1016/j.gca.2019.08.036
- 536 Kanbar, H.J., Montargès-Pelletier, E., Losson, B., Bihannic, I., Gley, R., Bauer, A., Villieras, F.,
537 Manceau, L., El Samrani, A.G., Kazpard, V., Mansuy-Huault, L. (2017). Iron mineralogy as a
538 fingerprint of former steelmaking activities in river sediments. *Sci. Tot. Environ.* 599-600, 540-553.
539 doi: 10.1016/j.scitotenv.2017.04.156
- 540 Kanbar, H. J. (2017). What the Orne River tells about the former steelmaking activities: chemical and
541 mineralogical investigations on sediments. PhD dissertation, Université de Lorraine, France.
- 542 Klaver, G., Verheul, M., Bakker, I., Petelet-Giraud, E., Négrel, P. (2014). Anthropogenic rare earth
543 element in rivers: gadolinium and lanthanum. Partitioning between the dissolved and particulate phases
544 in the Rhine River and spatial propagation through the Rhine-Meuse Delta (the Netherlands). *Appl.*
545 *Geochem.* 47, 186–197. doi: 10.1016/j.apgeochem.2014.05.020
- 546 Knobloch, V., Zimmermann, T., Gößling-Reisemann, S., (2018). From criticality to vulnerability of
547 resource supply: the case of the automobile industry. *Resour. Conserv. Recycl.* 138, 272–282. doi:
548 10.1016/j.resconrec.2018.05.027
- 549 Kulaksiz, S., Bau, M. (2013). Anthropogenic dissolved and colloid/nanoparticle-bound samarium,
550 lanthanum and gadolinium in the Rhine River and the impending destruction of the natural rare earth
551 element distribution in rivers. *Earth Planet. Sci. Lett.* 362, 43–50. doi: 10.1016/j.epsl.2012.11.033

- 552 Lachaux, N., Cossu-Leguille, C., Poirier, L., Gross, E.M., Giamberini L (2022)., Integrated
553 environmental risk assessment of rare earth elements mixture on aquatic ecosystems. *Front. Environ.*
554 *Sci.* 10:974191. doi: 10.3389/fenvs.2022.974191
- 555 Lodders, K. (1996). An experimental and theoretical study of rare earth element partitioning between
556 sulfides (FeS, CaS) and silicate and applications to enstatite achondrites. *Meteorit. Planet. Sci.* 31, 749–
557 766. doi: 10.1111/j.1945-5100.1996.tb02110.x
- 558 Losson, B., Manceau, L., Kanbar, H.J., Waldvogel, Y., Delus, C., Mansuy- Huault, L., Hissler, C.,
559 Montargès-Pelletier, E. (2020). Hydrodynamique de l'Orne et mobilisation sédimentaire dans la zone
560 de remous amont du barrage de Beth (Lorraine, France). *Géomorphologie : relief, processus,*
561 *environnement.* doi: 10.4000/geomorphologie.14004
- 562 Louis, P., Messaoudene, A., Jrad, H., Abdoul-Hamid, B.A., Vignati, D.A.L., Pons, M.-N. (2020).
563 Understanding rare earth elements concentrations, anomalies and fluxes at the river basin scale: the
564 Moselle River (France) as a case study. *Sci. Total Environ.* 742, 140619. doi:
565 10.1016/j.scitotenv.2020.140619
- 566 Martin, L.A., Vignati, D.A.L., Hissler, C. (2021). Contrasting distribution of REE and yttrium among
567 particulate, colloidal and dissolved fractions during low and high flows in peri-urban and agricultural
568 river systems. *Science of Total Environment* 790: 148207. doi: 10.1016/j.scitotenv.2021.148207
- 569 Martínez-Carreras, N., Ogorzaly, L., Walczak, C., Merlin, C., Montargès-Pelletier, E., Gantzer, C.,
570 Iffly, J.F., Cauchie, H.-M., Hissler, C. (2021). F-Specific RNA Bacteriophage Transport in
571 StreamWater: Hydro-Meteorological Controls and Association with Suspended Solids. *Water* 2021,
572 13, 2250. doi: 10.3390/w13162250
- 573 Merschel, G., Bau, M., Baldewein, L., Dantas, E.L., Walde, D., Bühn, B. (2015). Tracing and tracking
574 wastewater-derived substances in freshwater lakes and reservoirs: anthropogenic gadolinium and
575 geogenic REEs in Lake Paranoá, Brasilia. *CRGeosci.* 347, 284–293. doi: 10.1016/j.crte.2015.01.004
- 576 Parant, M., Perrat, E., Wagner, P., Rosin, C., Py, J.-S., Cossu-Leguille, C. (2018). Variations of
577 anthropogenic gadolinium in rivers close to waste water treatment plant discharges. *Environ. Sci.*
578 *Pollut. Res.* 25, 36207–36222. doi : 10.1007/s11356-018-3489-6
- 579 Picon, M. (2014). Autour de l'Orne industrielle: paysages industriels hérités. *Environmental*
580 *Engineering; Université de Lorraine.* <dumas-01110255>
- 581 Steinmann, M., Stille, P. (1997). Rare earth element behavior and Pb, Sr, Nd isotope systematics in a
582 heavy metal contaminated soil. *Appl. Geochem.* 12, 607–624. doi: 10.1016/S0883-2927(97)00017-6
- 583 Stille, P., Pierret, M.-C., Steinmann, M., Chabaux, F., Boutin, R., Aubert, D., Pourcelot, L., Morvan,
584 G. (2009). Impact of atmospheric deposition, biogeochemical cycling and water-mineral interaction on
585 REE fractionation in acidic surface soils and soil water (the Strengbach case). *Chem. Geol.* 264, 173–
586 186. doi: 10.1016/j.chemgeo.2009.03.005
- 587 Stille, P., Clauer, N. (1994). The process of glauconitization: chemical and isotopic evidence. *Contrib.*
588 *Mineral. Petrol.* 117, 253–262. doi: 10.1007/BF00310867

- 589 Taylor, S.R., McLennan, S.M., (1985). *The Continental Crust: Its Composition and Evolution*.
590 Blackwell, Oxford, 312p.
- 591 Tricca, A., Stille, P., Steinmann, M., Kiefel, B., Samuel, J., Eikenberg, J. (1999) Rare earth elements
592 and Sr and Nd isotopic compositions of dissolved and suspended loads from small river systems in the
593 Vosges mountains (France), the river Rhine and groundwater. *Chem. Geol.* 160, 139–158. doi:
594 10.1016/S0009-2541(99)00065-0
- 595 Vdović, N., Billon, G., Gabelle, C., Potdevin, J.-L., 2006. Remobilization of metals from slag and
596 polluted sediments (case study: the canal of the Deûle River, northern France). *Environ. Pollut.*
597 141:359–369. doi: 10.1016/j.envplo.2005.08.034
- 598 Zebracki, M. (2008). *Devenir des polluants métalliques associés aux sédiments contaminés dans un*
599 *cours d'eau en relation avec la dynamique sédimentaire*. PhD dissertation, Université Paris-Sud XI,
600 France.
- 601 Zhang, S., Ding, Y., Liu, B., Chang, C. (2017). Supply and demand of some critical metals and present
602 status of their recycling in WEEE. *Waste Manag.* 65, 113–127. doi: 10.1016/j.wasman.2017.04.003.

In review

Figure 1.JPEG

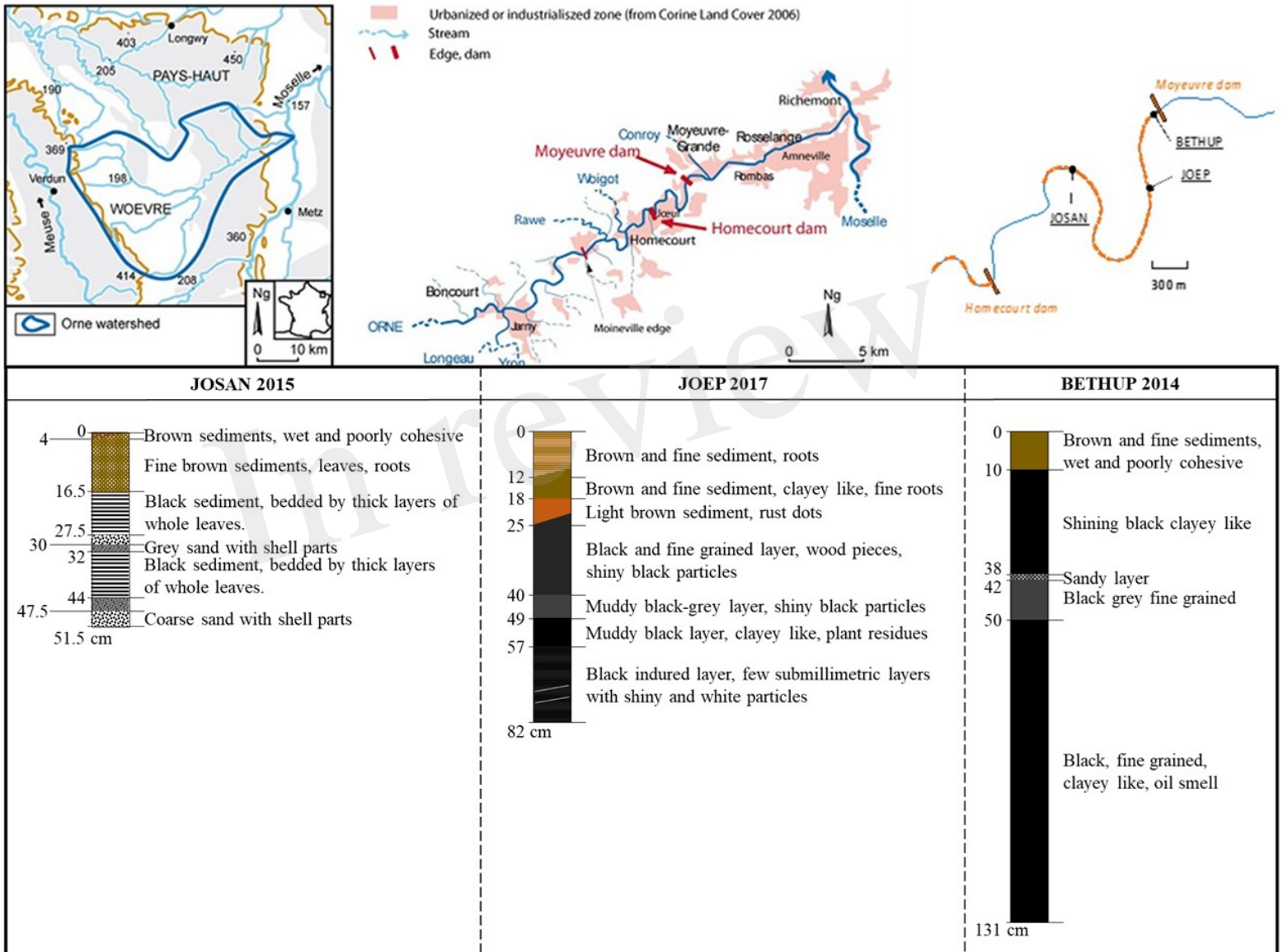


Figure 2.JPEG

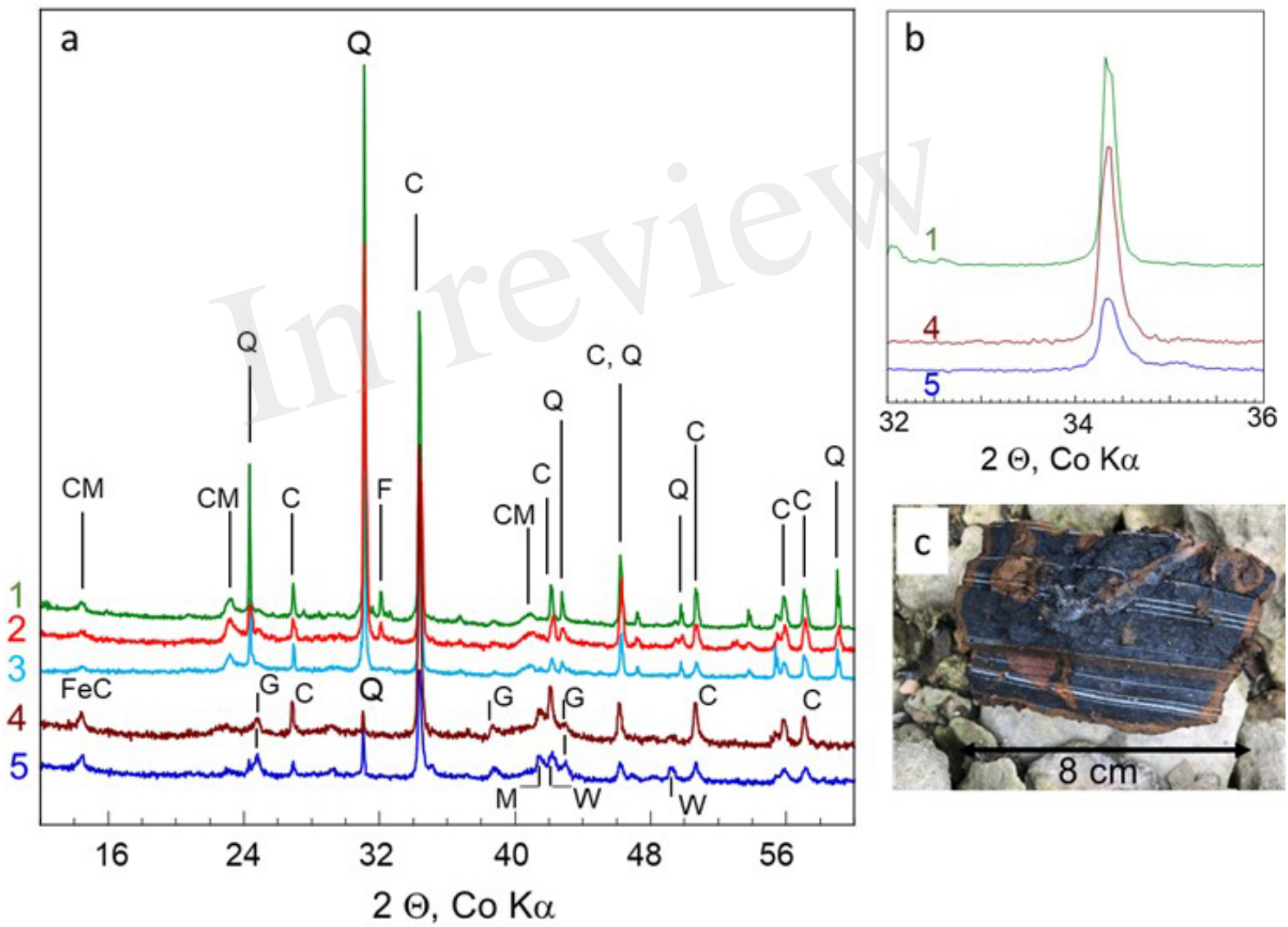


Figure 3.JPEG

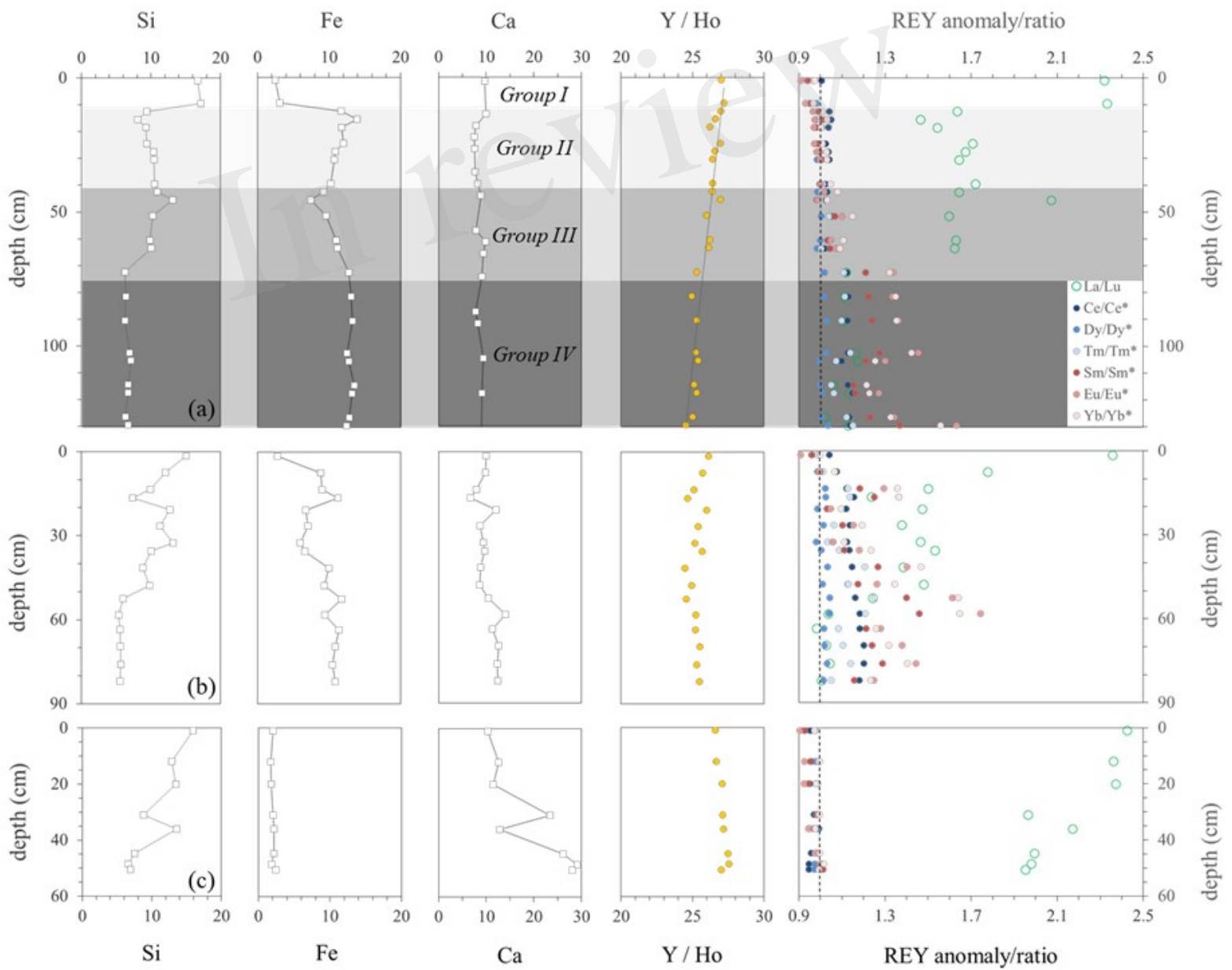


Figure 4.JPEG

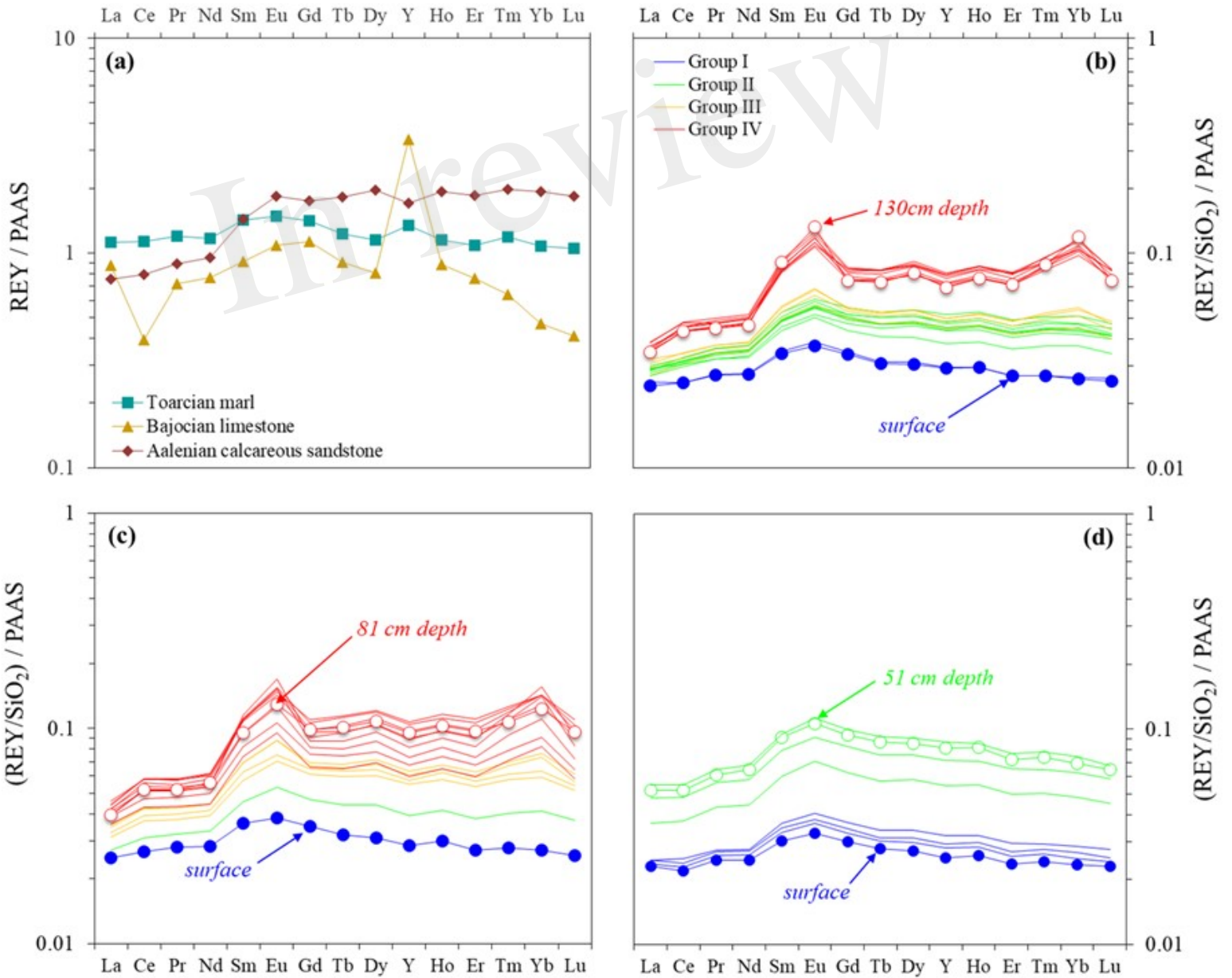


Figure 5.JPEG

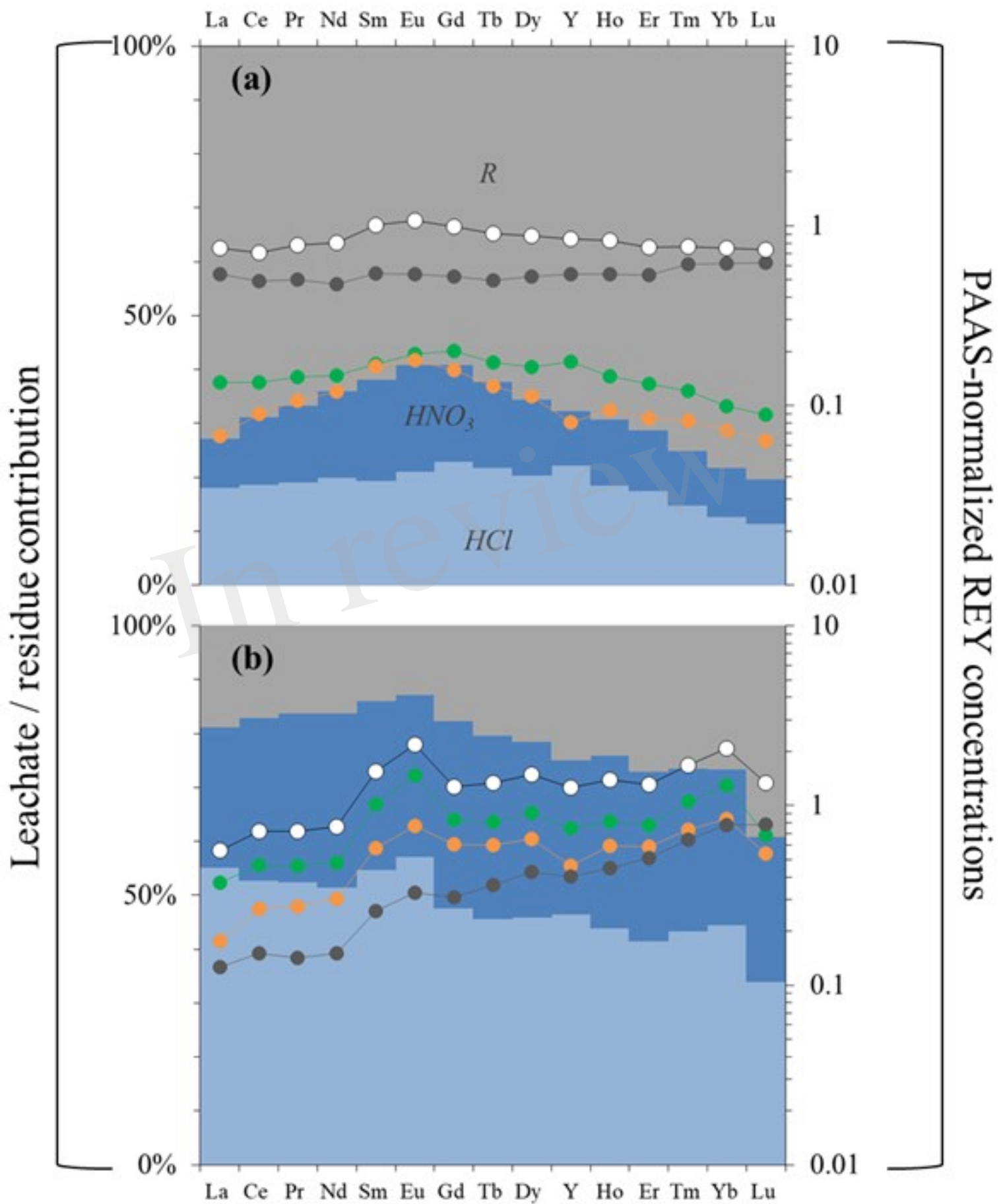


Figure 6.JPEG

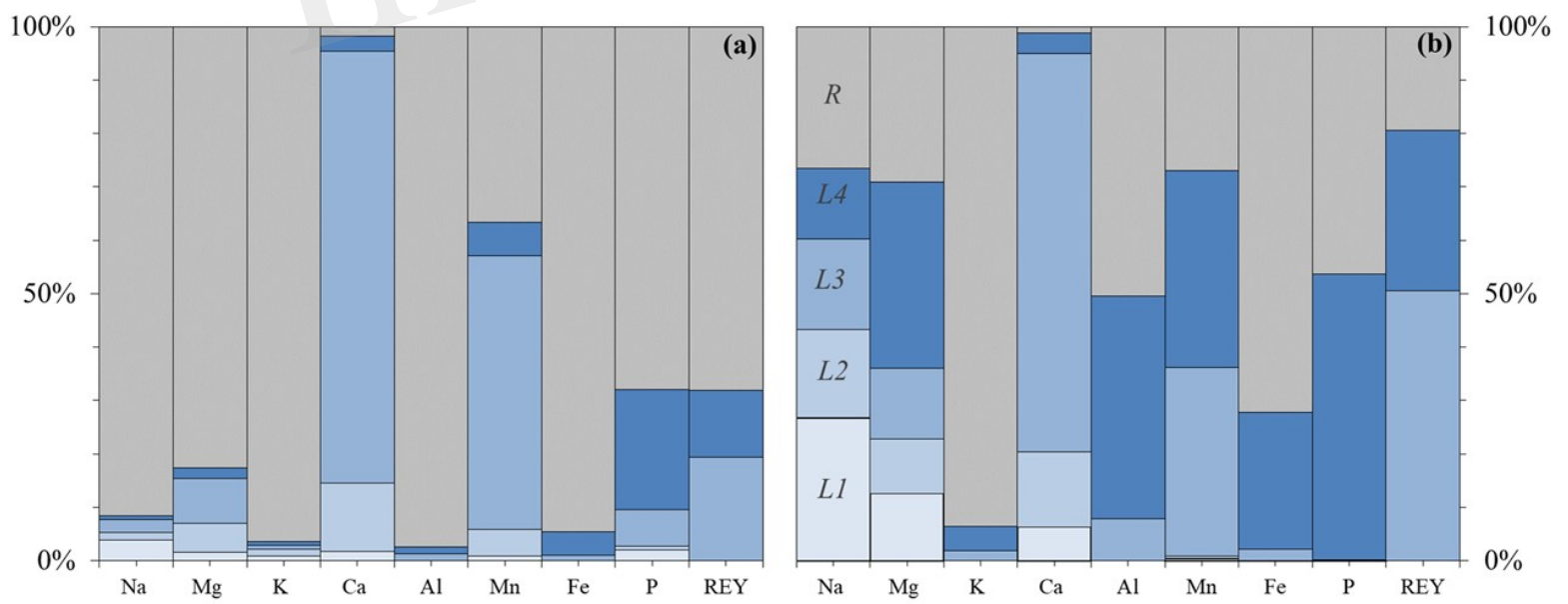


Figure 7.JPEG

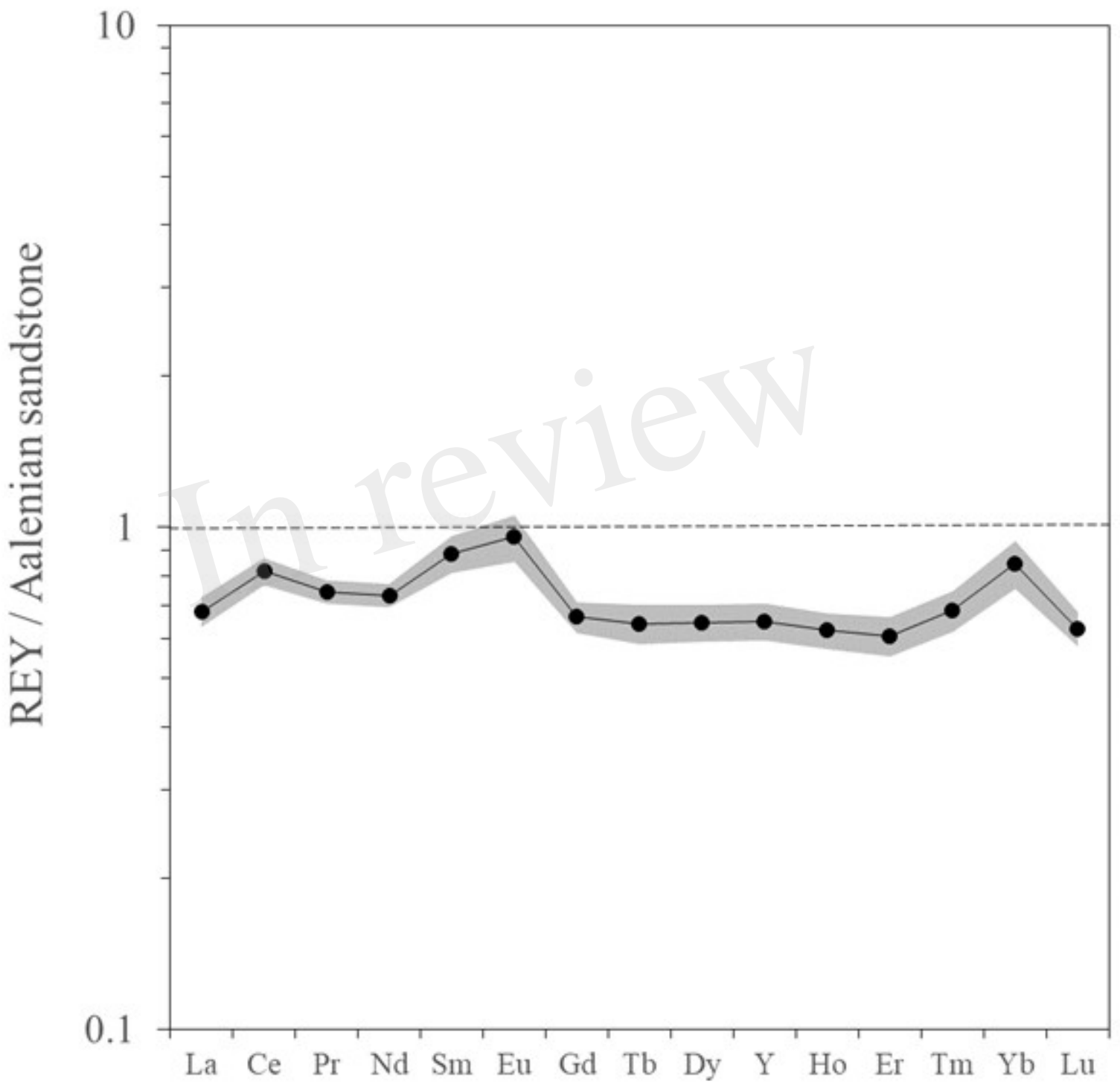


Figure 8.JPEG

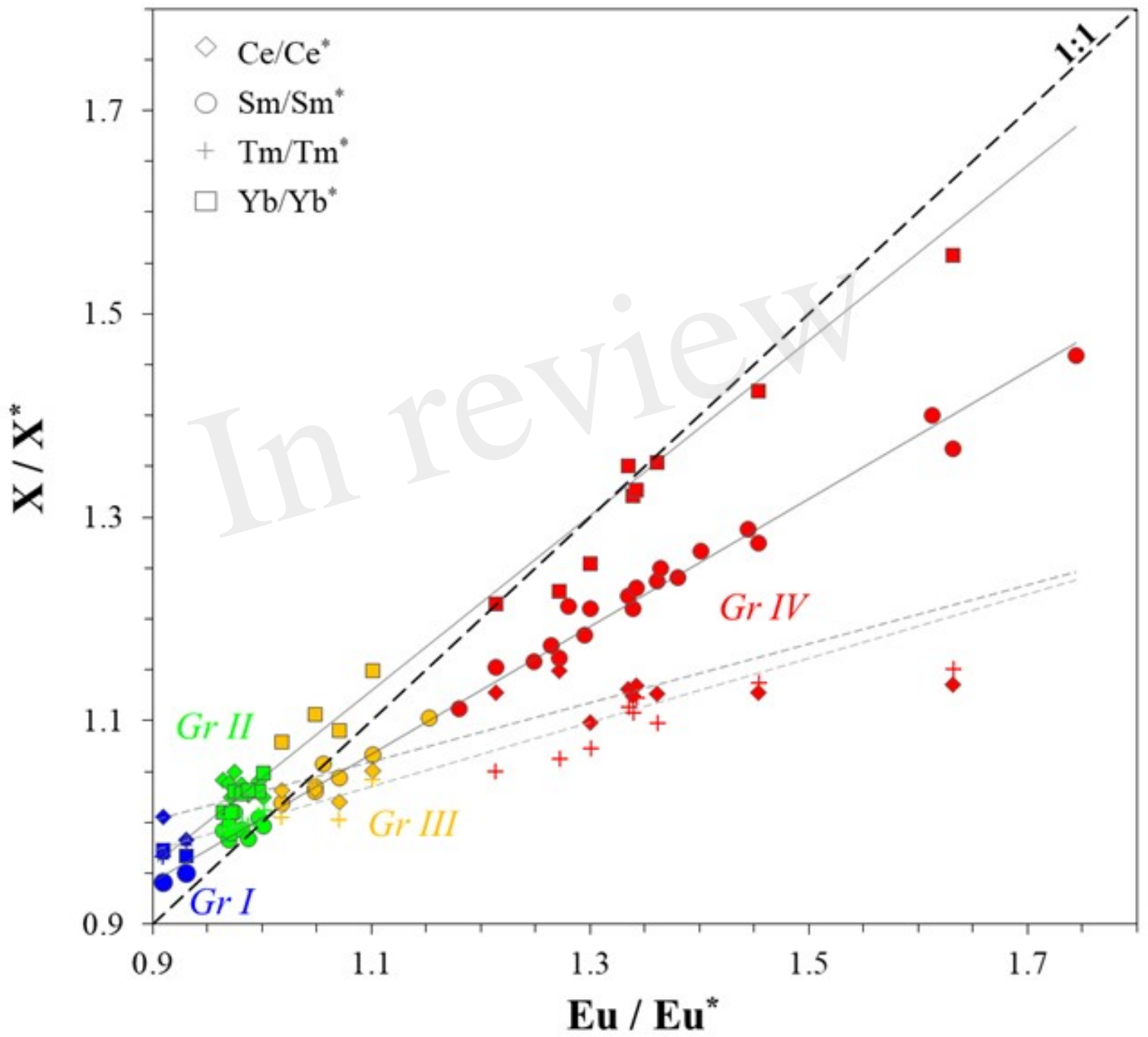


Figure 9.JPEG

